Numerical investigation of heat transfer and flow characteristics of a double-wall cooling structure: reverse circular jet impingement

Abdallah Ahmed[a,b], Edward Wright[a], Fawzy Abdel-Aziz[b], Yuying Yan[a]*

[a] Fluids & Thermal Engineering (FLUTE) Research Group, Faculty of Engineering, University of Nottingham, University Park, Nottingham, NG7 2RD, UK

[b] Mechanical Power Engineering Department, Faculty of Engineering, Cairo University, Giza, Egypt

*Corresponding: yuying.yan@nottingham.ac.uk

Abstract

Double-wall cooling structures are commonly used to enhance the heat transfer in combustor liner and aerofoil internal cooling within gas turbine engines and other industrial applications. This is the first study to adopt a novel reverse jet impingement technique into a double-wall cooling structure in order to achieve a higher heat transfer rate with relatively lower pressure drop. This paper uses the computational fluid dynamics to study crossflow, nozzle configuration, inlet orientation, and jet-to-target spacing distance effects on the heat transfer rate and the discharge coefficient. In this study, jet-to-target spacing was varied from 1.6 to 7 jet diameter, jet-to-jet spacing was 3.4 jet diameter, the reverse tube diameter was 3.2 jet diameter, and jet Reynolds number was set at 23,000. Procedural optimisation throughout the study initially evaluated that nozzles extended through the crossflow channel are more effective than the square-edged nozzles in eliminating the crossflow effect and promoting higher heat transfer. Variation of inlet condition yielded no significant optimisation was found. Jet-to-target spacing was optimised at jet-to-target spacing around 3 jet diameter. The most significant variable affecting nozzle discharge coefficient was the flow area of the outlet. The reverse jet impingement design showed capacity to enhance heat transfer by increasing the internal surface area, and minimise negative crossflow effects, without excessive reduction in the discharge coefficient.

Keywords: Double-wall cooling, jet impingement, reverse impingement, heat transfer

Nomenclature

Re	Reynolds number
H	Nozzle exit to target spacing
D_j	Nozzle diameter
S	Jet-to-jet spacing
δ	Dimple depth
h	Heat transfer coefficient
$\dot{q}$	Heat transfer rate
K	Thermal conductivity
$\dot{m}$	Air mass flow rate
n	Number of jets
ΔP	pressure drop
$\overline{Nu}$	Average Nusselt number
$\overline{\overline{Nu}}$	Total average Nusselt number
T	Air temperature
μ	Air dynamic viscosity
ρ	air density

Subscripts

j	Refers to jet
w	Refers to target wall

1. Introduction

Jet impingement has been used in many applications as a result of its high convective heat transfer rates, especially near the stagnation zone. Therefore, the jet impingement technique is widely used in a variety of applications and industries (i.e., gas turbine blades and combustion chamber cooling, aircraft wing de-icing, electronic component cooling, food processing, glass and metal tempering, paper drying, and textiles) [1], [2].

There are a large number of parameters which control the jet impingement performance, including jet shape, jet hydraulic diameter (D_j), jet angle, jet-to-target spacing (H/D_j), jet-to-jet spacing(S/D_j), jet arrangement, target surface curvature, dimple depth (δ/D_j), Reynold's number (Re), etc. There have been several numerical and experimental studies carried out on different impinging surface configurations to investigate the optimal performance of heat transfer, such as pin fin, rib roughened surface, and other shapes [3]–[5]. A dimpled surface has been found to achieve a factor of 1.8-2.8 in heat transfer enhancement, while the pressure drop increases by a factor of 1.3-2.9 relative to a flat channel target [6]–[8]. The local heat transfer of dimpled surfaces increases by creating strong secondary vortex pairs which promote the turbulence near the heat transfer surface [9]. In addition to, dimples increase the heat transfer surface area, as the surface area for a hemisphere shape equals two times the surface area of its cap. However, using turbulators in double-wall structures for heat transfer augmentation typically incurs a higher pressure loss penalty.

A detailed study on the influence of the jet impingement main parameters on the heat transfer and the flow characteristics (H/D_j = 1-12, δ/D_j = 0.15-0.25, Re = 5000-11,500) [10]. At H/D_j = 8, Re = 11,500), the dimpled surface heat transfer rate increased by 50% compared to the smooth surface. In the case of a deep dimpled surface with small jet-to-target spacing, H/D_j, there was a small decrease in heat transfer. In addition, the highest heat transfer has been obtained when the impinging jet was aimed at the dimple centre.

For large heat transfer areas, the multiple jets are utilised in the pattern of a row or array. However, the interaction between adjacent jets and the accumulated cross-flows from the upstream jets impact the heat transfer and flow characteristics of a multiple jet impingement arrangement by reducing the effectiveness of each jet. The optimum H/D_j range is one of the most significant differences between single and multiple jet impingement cases [11]. The optimum spacing distance between the nozzle exit and the target surface for single and multiple jet impingement cases often equals 5-6 D_j, 3-4 D_j, respectively. In-line and staggered jet impingement arrays were investigated experimentally [12], [13]. The in-line jets attained higher heat transfer rates than the staggered jets.

The jet-to-target spacing distance is responsible for the significant heat transfer rate deterioration at $H/D_j > 6$. The jet-to-jet spacing, S/Dj, greater than 4 showed the best uniform Nu distribution and the highest heat transfer rate.

The transient liquid crystal technique has been applied to study the heat transfer rate of jet impingement over a dimpled target. The influence of the dimple geometries, dimple location, and crossflow configuration were investigated [14]. The results revealed that the average Nu for a shallow dimple case was increased by 70% compared to the smooth target. Moreover, the pressure drop of the dimpled target case was of the same magnitude as the smooth surface.

The crossflow of a single spent flow outlet for an impinging jet array and its effect on the heat transfer rates in a channel with flat or curved impinging target were studied [15]–[17]. The impacts of Re and S/D_j on the heat transfer of a staggered jet array at S/D_j = 1.5-8 and Re = 8,200-52,000 were studied [18]. The heat transfer rates decreased due to the crossflow and the interfaces between the vortex structures that initially formed around the jets and then impinged with jet-to-jet interactions when they advected away the stagnation points over the impinging surface [19], [20].

Influence of the nozzle shapes, the heat transfer distribution over the target surface of jet impingement was investigated by testing two in-line jet arrays of square and circular nozzle shape [21], [22]. The impinging circular jet array gained 8% higher heat transfer rate than the square jet array. It was also noticed that for the circular jet arrays, the maximal local and average heat transfer rates occurred at jet-to-jet spacing distance, S/D_j, of 4.

Nozzle configuration also plays a main role in creating the initial flow velocity and turbulence intensity profiles at the nozzle outlet, consequently nozzle configuration can affect the heat transfer performance. Three different orifice nozzle configurations (i.e. the standard edged, sharp-edged, and square-edged nozzles) were experimentally studied for a circular jet impingement [23]. The square-edged orifice jet delivered the highest heat transfer rates at H/D_j= 2-4.

An in-line jet array with extended nozzles has been used to investigate experimentally the effectiveness of the extended nozzles for flat plate jet impingement [24], [25]. The results showed that the extended nozzles increased heat transfer rate by 40-50% compared with the sharp-edged nozzles.

After reviewing the previous studies, we can conclude that narrow crossflow channels reduce the interfacing between adjacent jets, but at the same time increase the accumulated crossflow velocity which reduces the heat transfer rate, especially for the jets in proximity to the spent air outlet. Moreover, there are constrains on the spacing distance between the adjacent jets and the spacing distance between jets nozzle to target surface for jet arrays to minimise the interaction between the adjacent jets. Accordingly, the main aim of this research was to investigate a new double-wall target surface structure to eliminate the heat transfer deterioration as a result of the crossflow. Moreover, improving the heat transfer rate by increasing the internal surface area without incurring excessive pressure loss. This new design is inspired by the reverse flame/thimble boiler, as the target surface is in the form of a thimble, with the impinging jet is concentrated down the centre. The air doubles-back on itself within the thimble to come to the front of the nozzle plate before exiting through the outlets.

2. The Physical Problem and Boundary Conditions

In this study, air is used to impinge on a thimbled target surface from five square-edge/extended pipe circular nozzles arranged in-line to form a row of reverse impingement jets, as shown in

Fig. **1**. Nozzle diameter is 25mm, the jet-to-jet spacing distance equals 3.4 D_j, the nozzle plate thickness and crossflow channel height equals 1 D_j. All nozzles are concentric with the five thimbles. The thimble structure consists of a hemispherical dimple and a hollow cylinder. Dimples and cylinders have the same diameter, D_d, which equals 3.2 D_j. The air mass flow rate is constant in all study cases to set the same average jet Reynolds number for all cases, Re=

23,000. The inlet and exit orientation, and the jet-to-target spacing distance are variable to assess how they affect heat transfer rate and flow characteristics.

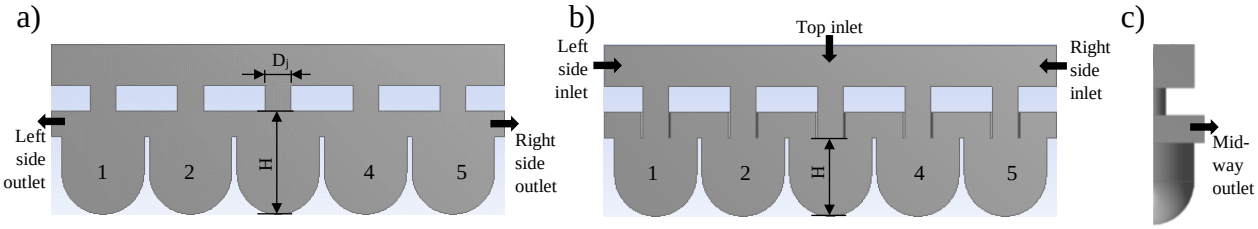

Fig. 1. Reverse jet impingement computational domain with different inlet and outlet configurations (a) square-edged nozzle (b) extended nozzle (c) side view.

Air temperature and turbulence intensity of the inlet conditions are adjusted to 298K and 10%, respectively. The outlet boundary condition is set to zero-gauge pressure. A constant heat flux of $\dot{q} = 1000\ W/m^2$ is applied at the target surface. Adiabatic conditions are applied for other walls, and all walls adapt the no-slip shear condition. **Table 1** summarises the nine study cases conducted in this study.

Table 1. Case studies and Parameters.

Case no.	Inlet	Outlet	Extended nozzle	H/D_j
1	T	R	-	4
2	T	L&R	-	4
3	T	M,L&R	-	4
4	T	R	✓	3
5	L	R	✓	3
6	R	R	✓	3
7	T	R	✓	1.6
8	T	R	✓	5
9	T	R	✓	7

T: top, L: left, R: right, M: midway

3. Numerical Procedure

With the aim of getting a comprehensive interpretation for the flow field and heat transfer in the reverse jet impingement cooling structure, the commercial CFD software ANSYS Fluent 19.2 has been used. Three-dimensional numerical computations have been carried out to solve the governing equations [26]. Coupled schemes for pressure-velocity coupling were used for better convergence. Air properties have been defined as a function in the air temperature. Convergence of the discretised equations was achieved when all the residuals of u, v, w, p, k, and ω were less than 10^{-4}, whilst for energy the residual target was less than 10^{-6}, alongside that the quantities of interest, such as average Nusselt number and inlet pressure, must become steady and not change through iterations.

Since the reverse jet impingement is a novel design, so there is a shortage in the published data for the reverse jet impingement. Thus, heat transfer of a single reverse jet impingement has

been experimentally investigated by using a wind tunnel with heated air and applying the Transient Liquid Crystal technique to validate the numerical work, as explained in the next two sections. The experimental test-rig setup has been illustrated particularly in previous work [27], [28].

3.1. Grid sensitivity

A grid independence study has been performed to confirm that the results are not dependent on the mesh resolution. Tetrahedral volume meshes were generated by ANSYS Meshing. Five meshing grids with consecutive element sizes of 1, 2, 3, 4, and 5mm have been used to check the grid independency. The thickness of the first meshing layer adjacent to the target surface is set to be 0.004 mm with expansion ratio of 1.2 to ensure that the maximum local value of the Y plus is less than 1.0, and the skewness value does not exceed 0.8 throughout the five grid resolutions. **Fig. 2** shows the investigated results of the dimple and the cylinder average Nu numbers, and the discharge coefficient for the five meshing grids. The extrapolation value for the infinitesimal grid (i.e., element size$\approx 0mm$) was calculated by applying the Richardson Extrapolation method [29]. Based on the extrapolated values of the infinitesimal grid, the deviation of the averaged dimple and cylinder Nu numbers and the discharge coefficient is less than 1% for the 1mm ,2mm ,3mm grids. Consequently, the 3mm grid has been adopted for the purpose of saving the computational time.

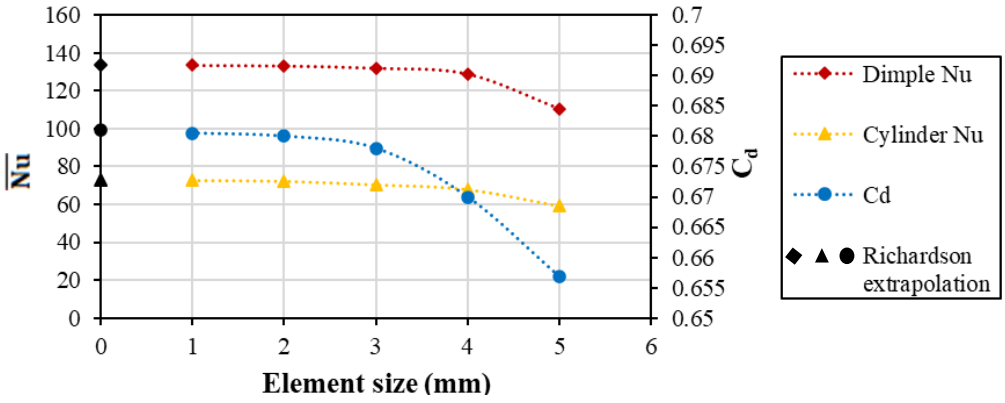

Fig. 2. Grid sensitivity analysis at element size 1,2,3,4 and 5mm.

3.2. Turbulence model

The standard k-ε [30], Realizable k-ε [31], standard k-ω [32], and SST k-ω [33] turbulence models have been used to evaluate their effectiveness in predicting the flow characteristics and heat transfer performance in the reverse jet impingement structure. **Fig. 3** shows the comparison between the numerical results of four turbulence models and the experimental results for the dimple average Nu. Generally, the trend of SST k-ω results is closest to the observed experimental results trend amongst the other turbulence models. In addition, the results of SST k-ω turbulence model at $H/D_j = 4$ and 6 are very close to the experimental values. Therefore, the SST k-ω model has been selected owing to its effectiveness in predicting the reverse jet impingement heat transfer performance. It is worth mentioning that the SST k-ω turbulence model has been extensively used in previous studies [34]–[37].

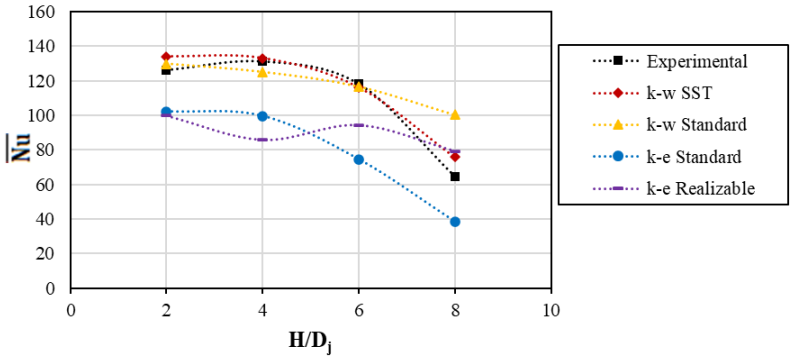

Fig. 3. Comparison of four turbulence models numerical results with experimental.

3.3. Definition of parameters

Data gained from the numerical computations were reduced by means of local Nusselt number, Reynolds number, and discharge coefficient.

Nusselt number, Nu, is defined as the ratio of convective heat transfer to conductive heat transfer and can be defined as the following:

$$Nu = \frac{\dot{q}.D_j}{(T_w - T_j).K} \tag{1}$$

where q̇ is the heat flux, D_j is the nozzle hydraulic diameter, T_w and T_j represent the target surface temperature and air jet temperature respectively, and K is the air thermal conductivity.

Reynolds number, Re, is the ratio of inertial forces to viscous forces. In the case of multiple jets, Reynolds number is calculated based on the total flow rate as a bulk-average, and the discrepancy between the individual jets is not considered. It can be defined as the following:

$$Re = \frac{4.\dot{m}}{n.\pi.D_j.\mu} \tag{2}$$

where $\dot{m}$ is the total air mass flow rate, n is the number of the jet nozzles, and μ is the air dynamic viscosity.

Discharge coefficient, C_d is defined as the ratio of the actual discharge to the theoretical discharge. It can be defined as follows:

$$C_d = \frac{4.\dot{m}}{n.\pi.D_j^2.\sqrt{2.\rho.\Delta P}} \tag{3}$$

Where, ρ is the air density of the fluid, and ΔP is the pressure drop across the jet impingement nozzle structure.

4. Results and Discussion

4.1. Effect of crossflow

To initially determine the effects of crossflow in the novel reverse jet impingement geometry, the standard sharp square-edged nozzles, and top inlet condition was tested with the three outlet

crossflow conditions. The resultant Nu number distributions were split into two sections, those observed on the target concave ‘dimple’, and those found on the cylindrical side wall ‘cylinder’ surface as shown in **Fig. 5** and Fig. 5 for local and average Nu distribution, respectively. This was done to understand how their separate mechanisms contribute towards the overall cooling effect.

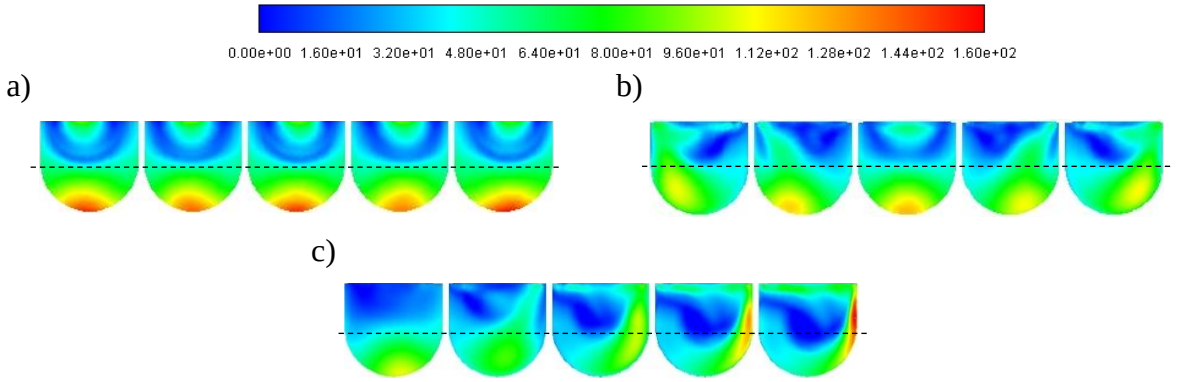

Fig. 4. Local Nu number distribution at different crossflow strengths: a)Minimum, b) Intermediate and c) Maximum.

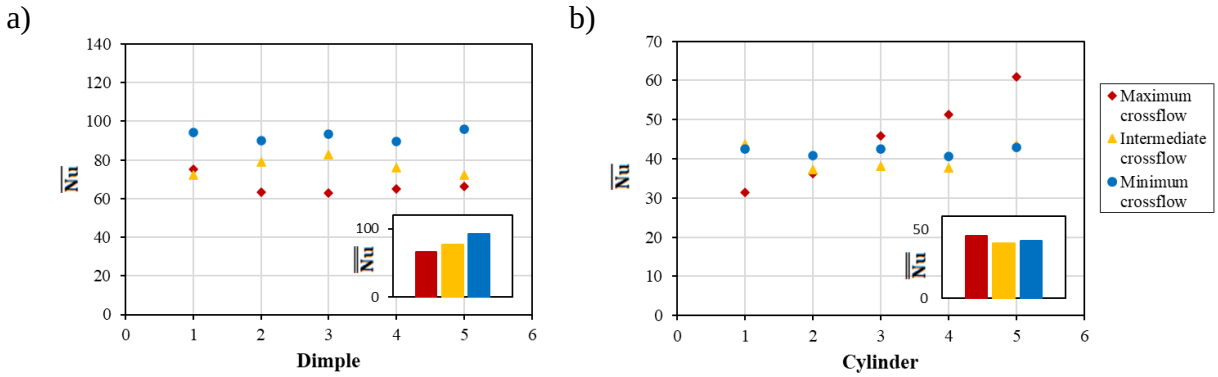

Fig. 5. Effect of crossflow on surface average Nusselt number: a) Dimples and b) Cylinders.

Firstly, the target ‘dimple’ is subjected to the impingement jet’s stagnation region, and is therefore the area of highest heat transfer, the flow then begins to develop radially outwards and flows perpendicular to the surface of the ‘cylinder’ as it travels towards the outlets. Concentrating specifically on the ‘dimple’ heat transfer surface, it can be observed that when cross flow is increased, average heat transfer across the whole array is reduced by 17%, and 28%, for the intermediate and maximum crossflow conditions respectively. Although we do see this average reduction when crossflow is present, relatively little Nu variation between each of the five ‘dimples’ is seen, especially in the minimum crossflow condition, where deviation is uniform, and below 2%. This heat transfer uniformity between individual jets for the minimum crossflow condition can be easily understood from velocity contours shown in **Error! Reference source not found.** a. In the intermediate crossflow condition, the highest heat transfer is observed in the central, 3rd jet, with subsequent jet Nu decreases of ≈7% for each jet towards the crossflow exits. This can again be predicted from the velocity flow fields shown in **Error! Reference source not found.** b.

In the maximum crossflow case, highest heat transfer is seen in jet 1, which is subjected to the least crossflow, but jets 2 through 5, a deviation of just 2.3%, and no general decrease is seen

in ‘dimple’ heat transfer as crossflow increases towards the outlet. This lack of diminished heat transfer is likely due to an inversely proportional relationship between two contributing factors two factors. Firstly, it is clear that an increased crossflow, as seen in subsequent jets, deflects the jet away from the stagnation point at the ‘dimple’ concave, this causes a reduction in Nusselt number. The second effect, which negates this loss, is that due to the location of the outlet, a pressure gradient is formed within the target cavity, decreasing from jet 1 to 5. Towards jet 4 and 5, this causes a larger pressure-drop over the nozzle, resulting in a larger velocity, and therefore Reynolds number. Naturally, the effect of this increased jet Re is a subsequently increased Nu. When the exit is arranged to the right of the test section, the combined the effects of the crossflow, and jet to jet Re variation mitigate each other, resulting in this ‘dimple’ heat transfer (**Error! Reference source not found.** c).

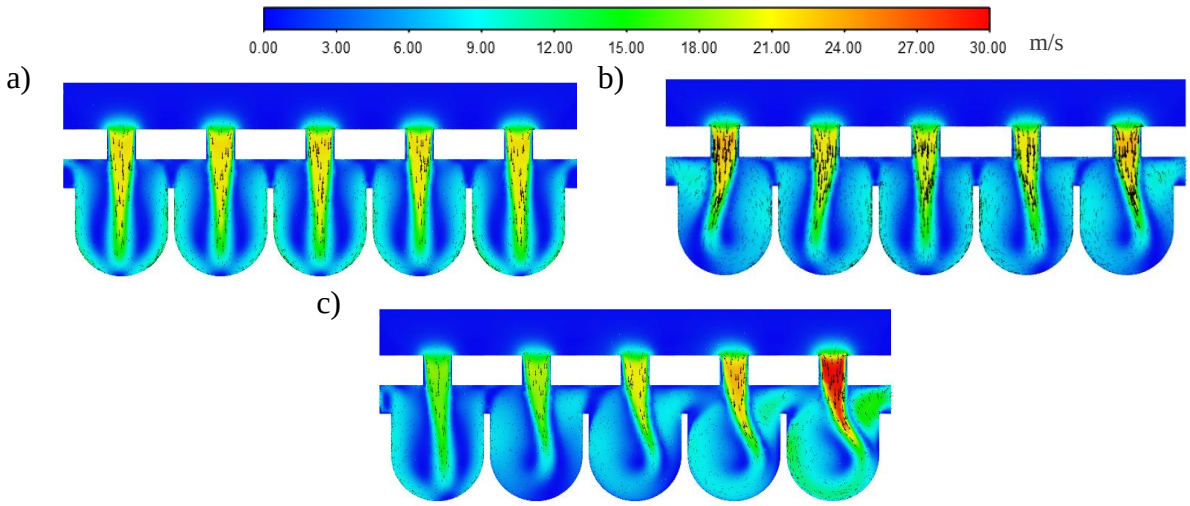

Fig. 5. Velocity contours at different crossflow strengths: a)Minimum, b) Intermediate and c) Maximum.

After impinging on the ‘dimple’ surface, the air then flows towards the exits, and across ‘cylinder’ side walls where it performs further heat transfer. Compared to the initial impingement mechanism, the slightly cooler fluid now develops a thicker boundary layer against the wall, resulting in a lower average Nu for this surface, reflected in the difference between ‘dimple, and ‘cylinder’ average Nu values seen in **Fig. 5**.

Although the ‘cylinder’ Nu is lower in magnitude by 46% than against the ‘dimple’, the average heat transfer for both intermediate and minimum crossflows show a similar relationship (Fig. 3). Both the minimum crossflow case and the intermediate case once again show very uniform Nu amongst jets, with the intermediate case now showing very similar, but opposite Nu increases of ≈7% for subsequent jets towards the crossflow direction. As previously discussed, the impinging jets closest to the crossflow outlets are slightly deflected, moving the impingement effect from the concave ‘dimple’ centre and towards the ‘cylinder’ walls (Fig. 5).

An analysis of the ‘cylinder’ wall heat transfer in the maximum crossflow case shows a significantly different heat transfer effect. It is found that the average Nu increases significantly towards crossflow direction (Fig. 3). With average Nu increasing 93% from jet 1 to 5. At jet 5 it is observed that the ‘cylinder’ average Nu is only 9% lower than that of the ‘dimple’. The analysis shows that the relatively high Nu in this region is caused by jet deflection towards

sidewall, and the increased Re previously discussed, shown in **Error! Reference source not found.** c, and a large swirl effect. This swirl effect is caused by the displacement of the jet from the centre, causing the jet to flow along the right-hand of the 'cylinder' wall, around the 'dimple' concave, and back up the left-hand wall, forming a large eddy, before exiting. This circular path causes the flow against the 'cylinder' wall to have a relatively large velocity, Re, and there for Nu compared to the typical case where impingement initially causes a localised stagnation.

4.2. Effect of nozzle configuration

To reduce the crossflow effects observed with the basic, sharp edged nozzle, the nozzle was extended to be level with the crossflow channel. The extended nozzles generally show exception effectiveness at eliminating the effects of crossflow on Nu as shown in **Fig. 6**.

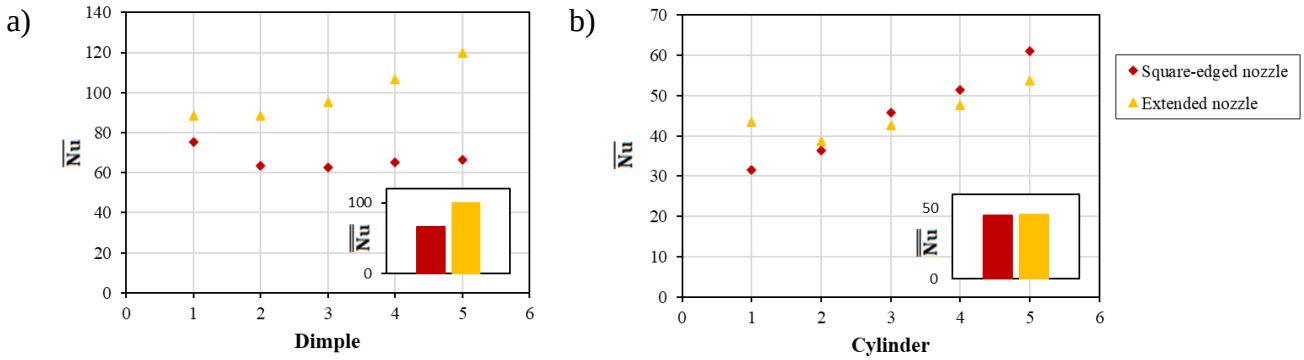

Fig. 6. Effect of nozzle configuration on Nu at maximum crossflow: a) Dimples b) Cylinders.

During this batch of testing, a top inlet condition, and right side outlet condition was set as an example of typical arrangement. This naturally creates a higher ΔP over the jet nozzles in proximity to the outlet. The variation in ΔP between jets generally results in a higher Re and therefore higher Nu in subsequent jets from 1 to 5.

When utilising the basic, sharp-edged nozzle, this ΔP effect is offset by the cumulative diminishing effects of crossflow from jets 1 to 5 as shown in **Fig. 7**, resulting in a relatively level Nu observed between the 5 jet 'dimple' targets. In this case, closer analysis of the 'cylinder' surfaces reveal that subsequent crossflow effects deflect the jet core from its natural target at the dimple, and accelerates the flow towards the 'cylinder' walls. The deflection causes an observed increasing in 'cylinder' wall Nu from jets 1 to 5, to the detriment of the 'dimple' surface heat transfer.

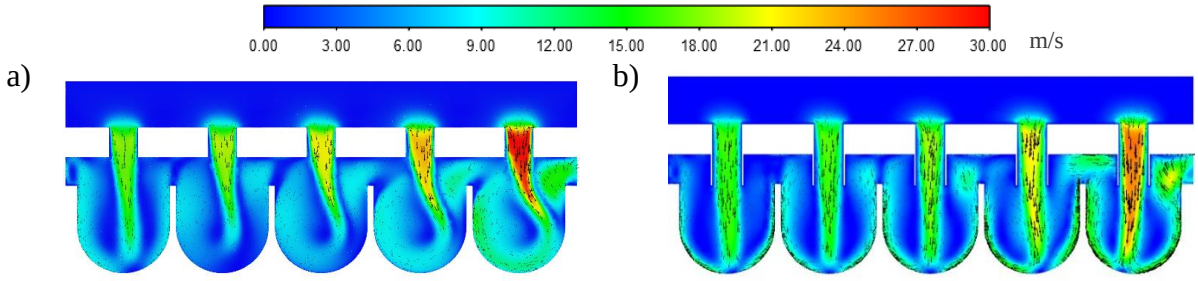

Fig. 7. Velocity contours for different nozzle configurations: a) Square-edged nozzles and b) Extended nozzles.

At the dimple surface, the extension of the nozzle geometry provides an average increase of 50% to the target surface (**Fig. 6** a). The ΔP effect which causes higher observed Nu of jets in proximity to the outlet is unaffected by the nozzle extension, but crossflow effects are almost entirely eliminated. Therefore, the most dramatic increase in Nu is observed jets closest in proximity to the outlet location, although it is noted that all jets see a Nu increase.

The positive effect of the extended nozzle on the 'cylinder' wall heat transfer is counteracted by a reduction in the crossflow 'deflection' of the jet towards the 'cylinder' walls (**Fig. 6** b). As the extended nozzle jet's effect is primarily aimed at increasing the target 'dimple' surface Nu, the observable increase in Nu at the 'cylinder' walls is a fraction of 1%, and is therefore not statistically significant.

The extended nozzle showed an exceptional ability to mitigate crossflow effects, and resulted in an overall increase of 50% over the basic nozzle design.

4.3. Effect of inlet configuration

To assess the effect of inlet configuration on the extended nozzle, simulation was conducted with variations in inlet direction, with the air either entering from the top, left side, or right-side inlet. All simulations were tested with pipe type nozzle, and the 'maximum crossflow case, where all air exits from the right-side outlet.

In all cases, the highest Nu is observed on the target section, with mean Nu values on the cylinder being 47.4% lower on average. Both the dimple and cylinder surface generally show higher Nu values in subsequent jets towards the crossflow direction due to the ΔP effect.

In all configurations and locations, jet 5 achieved the highest Nu due to its relatively high Re as shown in **Fig. 8**. This enhanced Re was caused by the ΔP effect from its proximity to the outlet, especially in the case where the high pressure inlet is also in proximity. The 'left side' inlet, 'right side' outlet case, has the most simple flow path, with a pressure gradient generally decreasing from left to right, and through the jets as shown in **Fig. 9** b. This more even pressure gradient results in a marginally increased average Nu, but still creates highest Nu values towards jet 5, the explanation for a lack of high Nu at jet 1 in proximity to the inlet is caused by an increased crossflow over the jet 1 nozzle inlet in the main plenum [27], [28].

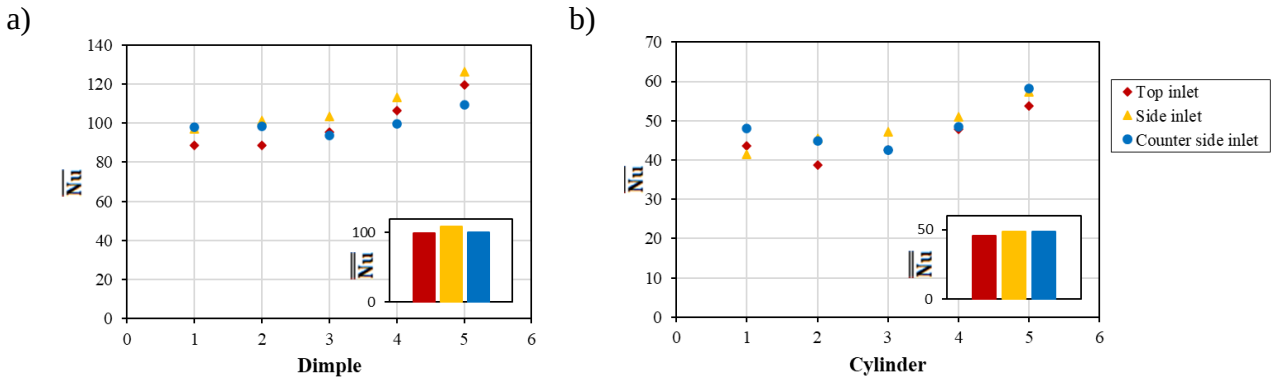

Fig. 8. The effect inlet direction on surface average Nu number: a) Dimples and b) Cylinders.

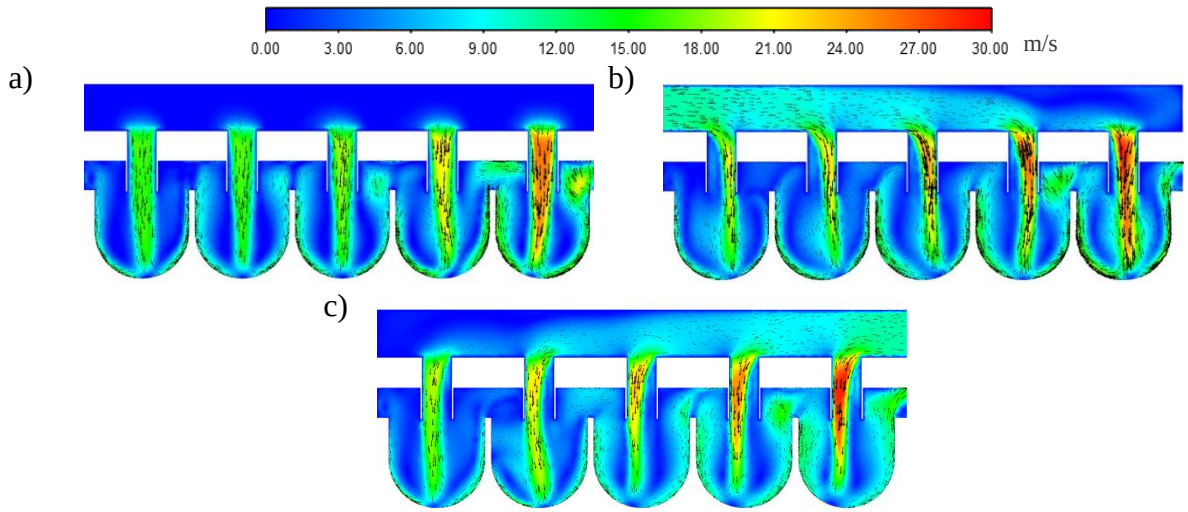

Fig. 9. Velocity contours for different inlet configurations: a) Top side, b) Left side and c) Right side.

None of the three inlet variations showed significant advantage. The left side entry resulted in marginally higher average Nu values due to the simplicity of the flow path from the left side inlet, to the right side outlet.

4.4. Effect of jet-to-target spacing

The final optimisation considered was the effect of distance between the nozzles and target surface, study was conducted to assess its effect on the heat transfer in this geometry arrangement. For this study, the independent variable was the jet-to-target spacing, therefore the 'pipe' type nozzle was used, with constant, typical 'top' inlet, and 'maximum crossflow' right side outlet conditions. Four variations of H/D_j were used, at H/D_j = 7, 5, 3, and the theoretical minimum of H/D_j = 1.6, where 'cylinder' wall length is set to 0, and only the dimple remains.

Assessment of the Nu distribution at the 'dimple' surface for H/D_j = 1.6, 3, and 5 conformed to the general trend of increased Re, and therefore Nu in the crossflow direction as shown in **Fig. 10** a and **Fig. 11**. The H/D_j = 7 case resulted in significantly lower Nu values, with diminishing heat transfer in the crossflow direction, analysis of the flow shows that the potential core of the jet was unable to effectively stagnate at the 'dimple' target surface at jet 1, with crossflow deflection of subsequent jets diminishing this ability further. Some diminishment effect was also observed in the H/D_j = 5 case, but this relatively insignificant.

a) b)

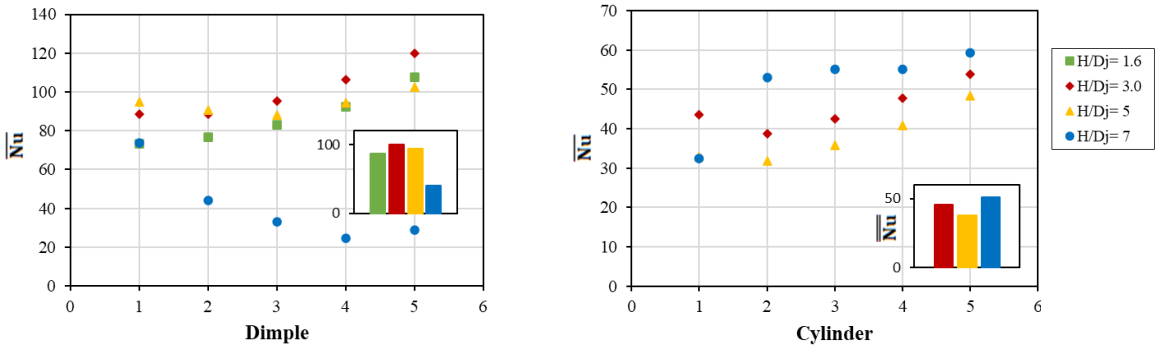

Fig. 10. Effect of H/D variation on surface averaged Nu number: a) Dimples and b) Cylinders.

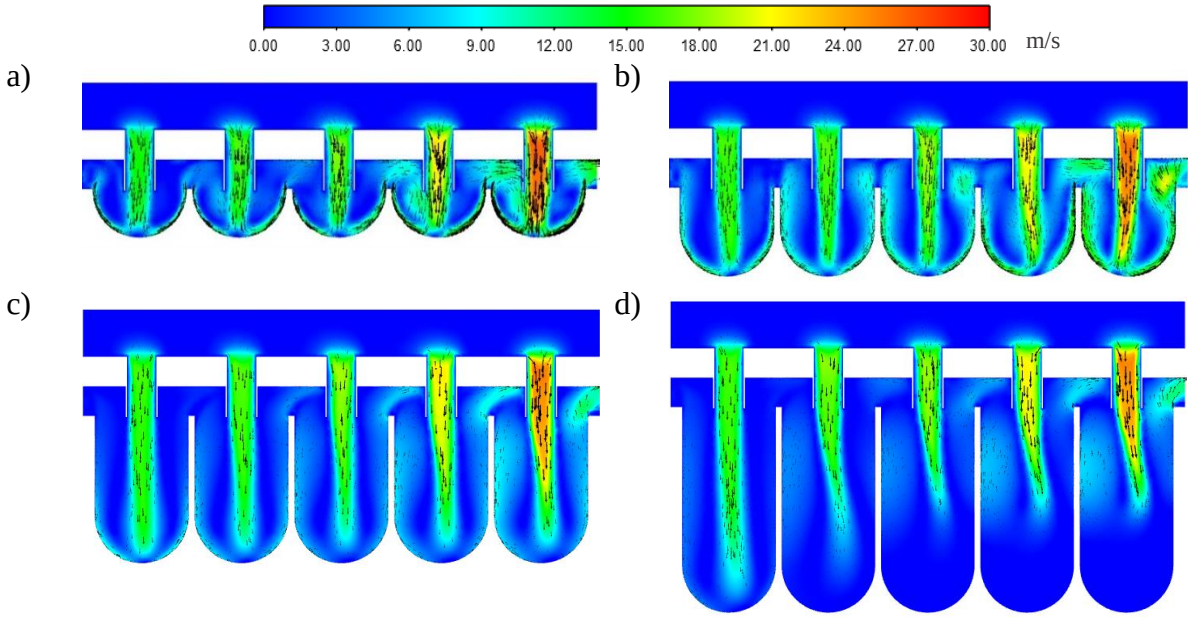

Fig. 11. Velocity contours at different H/D_j: a) H/D_j=1.6, b) H/D_j=3, c) H/D_j=5 and H/D_j=7.

Optimal impingement heat transfer against the 'dimple' surface was observed at H/D_j = 3, with average Nu 15%, 6%, and 144% higher than H/D_j = 1.6, 5, and 7 respectively. This suggests an optimal core length around the H/D_j = 3 jet-to-target range.

When considering the additional heat transfer contributed by the 'cylinder' wall portion of the reverse jet impingement geometry, it is important to note that a larger heat transfer surface will promote higher levels of total heat transfer. Average 'cylinder' wall values for Nu were taken, and are generally observed to be around half the magnitude of those over the 'dimple' regions. Due to the lack of target surface impingement stagnation in the H/D_j = 7 case, it is expected that this case witnesses the highest velocity flow against the 'cylinder' walls, resulting in a higher localised heat transfer, especially where the jet is deflected from its centreline.

Combining the effects of 'dimple' and 'cylinder' surface heat transfer, the H/D_j = 3 case is observed to produce the optimal overall heat transfer from the range chosen.

4.5. Pressure drop

A final numerical study was conducted to obtain discharge coefficient values for the potential flow combinations of the geometry. **Fig. 12** a, demonstrate that an increase in outlet flow area leads to increase in C_d. **Fig. 12** b, illustrates that modification of the inlet location demonstrate

very little effect on C_d. With the top inlet condition highest, and the counter side inlet, the lowest.

Very little difference in discharge coefficient is seen with a variation in H/D_j as shown in **Fig. 12** c, with slightly higher C_d observed with increasing the H/D_j, due to less interference from the typically high pressure stagnation zone generated at lower H/D_j values.

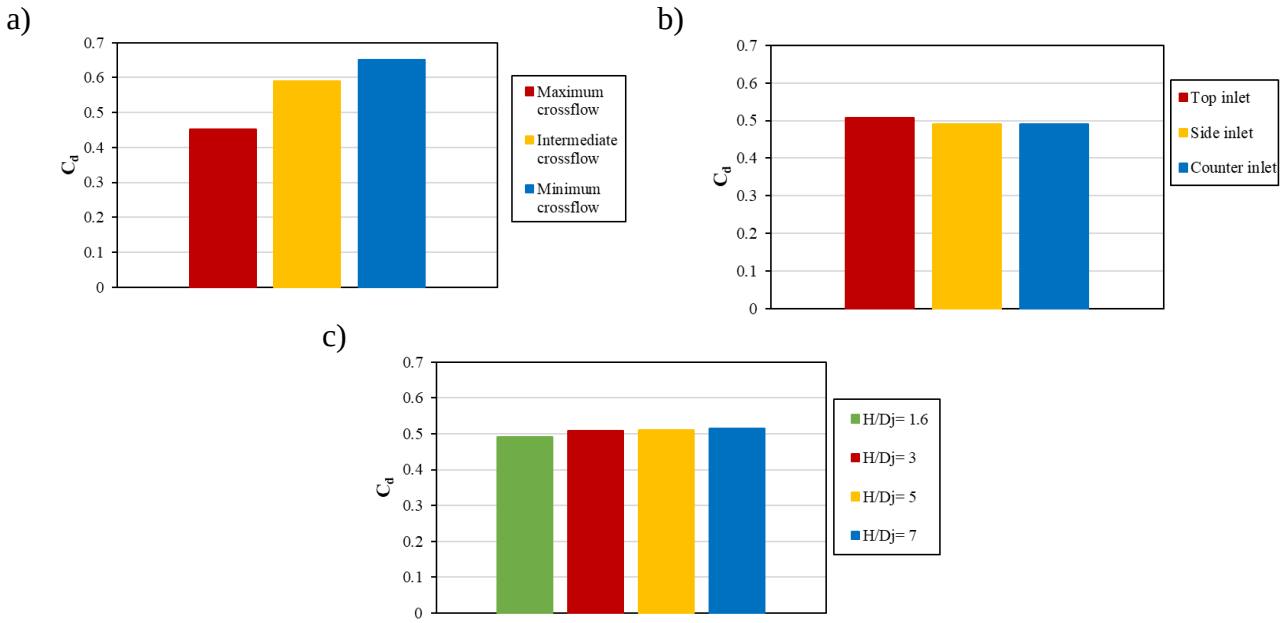

Fig. 12. Effects of (a) Outlet resultant crossflow (b) Inlet condition, and (c) H/D variation, on the resultant average jet nozzle discharge coefficient.

5. Conclusion

A novel reverse jet impingement geometry was analysed using CFD methodology. During procedural optimisation of the arrangement, variations of inlet, and nozzle geometry, and outlet conditions were tested to improve is effectiveness.

- Initial testing showed that crossflow effects were still significant in this geometry.
- Extension of the nozzle to the level of the crossflow channel significantly reduced the effect of crossflow and increased average Nu.
- Variation of inlet condition was analysed in depth, but no significant optimisation was found.
- Nozzle to target spacing was optimised at jet-to-target spacing around three jet diameter.
- When analysing nozzle discharge coefficient, the most significant variable was outlet condition, where a maximum flow area generated highest discharge coefficient.

This numerical study concluded that the current optimised reverse jet impingement arrangement utilises an extended nozzle. This design is highly resilient to the effects of crossflow, and therefore can be utilised with a range of inlet and outlet conditions.

Acknowledgement

The authors wish to acknowledge the University of Nottingham for providing access to the University's Augusta high performance computer. Also, we are grateful for this work supported by the IDB Merit Scholarship Programme, and EU H2020-MSCA-RISE-778104–ThermaSMART.

References

[1] X. Yang, Z. Liu and Z. Feng, "Effect of Film Extraction on Impingement Heat Transfer Characteristics of Jet Arrays on Spherical-Dimpled Surfaces," *Proceedings of the ASME Turbo Expo 2015: Turbine Technical Conference and Exposition*. *Volume 5A: Heat Transfer*. Montreal, Quebec, Canada. June 15–19, 2015.

[2] L. M. Wright, M. F. Malak, D. C. Crites, M. C. Morris, V. Yelavkar and R. Bilwani, "Review of Platform Cooling Technology for High Pressure Turbine Blades." *Proceedings of the ASME Turbo Expo 2014: Turbine Technical Conference and Exposition*. *Volume 5B: Heat Transfer*. Düsseldorf, Germany. June 16–20, 2014.

[3] D. H. Lee, Y. S. Chung, and P. M. Ligrani, "Jet Impingement Cooling of Chips Equipped With Multiple Cylindrical Pedestal Fins. " *ASME. J. Electron. Packag*.; 129(3): 221–228, September 2007.

[4] Y. Xing and B. Weigand, "Experimental investigation of impingement heat transfer on a flat and dimpled plate with different crossflow schemes," *Int. J. Heat Mass Transf.*, vol. 53, no. 19–20, pp. 3874–3886, 2010.

[5] E. J. Walsh and M. Mclean, "Heat Transfer From Novel Target Surface Structures to a Normally Impinging, Submerged and Confined Water Jet," *ASME. J. Thermal Sci. Eng. Appl*., vol. 1, no. 031001 , September 2009.

[6] G. I. Mahmood and P. M. Ligrani, "Heat transfer in a dimpled channel : combined influences of aspect ratio , temperature ratio , Reynolds number , and flow structure," *Int. J. Heat Mass Transf.*, vol. 45, no. 2002, pp. 2011–2020, 2001.

[7] M. L. Hill and D. L. Nelson, "Local Heat Transfer and Flow Structure on and Above a Dimpled Surface in a Channel," *ASME. J. Thermal Sci. Eng. Appl*., vol. 123, pp. 115–123, January 2001.

[8] N. K. Burgess and P. M. Ligrani, "Effects Of Dimple Depth on Channel Nusselt Numbers and Friction Factors," *ASME. J. Thermal Sci. Eng. Appl*., vol. 127, pp. 839–847, August 2005.

[9] P. Ligrani, "Heat transfer augmentation technologies for internal cooling of turbine components of gas turbine engines," *Int. J. Rotating Mach.*, vol. 2013, pp. 1-23, 2013.

[10] D. Zhang, "Flow and Heat Transfer Characteristics of Single Jet Impinging on Dimpled," *ASME. J. Thermal Sci. Eng. Appl*., vol. 135, 2013.

[11] F. Jets, "Nusselt-Reynolds Prize Paper Heat Transfer to Impinging Isothermal Gas and Flame Jets," *Experimental Thermal and Fluid Science J.*, vol. 6, pp. 111–134, 1993.

[12] L. W. Florschuetz, D. I. Takeuchi, and R. A. Berry, "Heat Transfer Characteristics for Inline and Staggered Arrays of Circular Jets with Crossflow of Spent Air," *J. of Heat Transfer-transactions of The ASME*., vol. 101, pp. 526–531, August 1979.

[13] S. Huang, J. D. Maltson, and Y. Y. Yan, "Experimental study on heat transfer improvement structures with staggered transverse elongated pedestal array," *Int. J. Heat Mass Transf.*, vol. 97, pp. 502–510, 2016.

[14] K. Kanokjaruvijit, "Heat Transfer and Pressure Investigation of Dimple Impingement," *ASME. J. Turbomach*., vol. 130, pp. 1–11, January 2008.

[15] B. Yang *et al.*, "Experimental and numerical investigation of heat transfer in an array of impingement jets on a concave surface," *Applied Thermal Engineering.*, vol 127, no. 25, pp. 473-483, 2017.

[16] P. M. Ligrani, Z. Ren, and W. C. Buzzard, "Impingement jet array heat transfer with small-scale cylinder target surface roughness arrays," *Int. J. Heat Mass Transf.*, vol. 107, pp. 895–905, 2017.

[17] W. C. Buzzard, Z. Ren, P. M. Ligrani, C. Nakamata, and S. Ueguchi, "Influences of target surface small-scale rectangle roughness on impingement jet array heat transfer," *Int. J. Heat Mass Transf.*, vol. 110, pp. 805–816, 2017.

[18] J. Lee, J. Haegele, P. Ligrani, and M. D. Fox, "Effects of Jet-To-Target Plate Distance and Reynolds Number on Jet Array Impingement Heat Transfer," *ASME. J. Turbomach.*, vol. 136, no. 5, pp. 1–13, May 2014.

[19] A. Terzis, "On the correspondence between flow structures and convective heat transfer augmentation for multiple jet impingement," *Exp. Fluids*, vol. 57, no. 9, pp. 1–14, 2016.

[20] A. Terzis, P. Ott, and M. Cochet, "Heat transfer characteristics of high crossflow impingement channels : Effect of number of holes," *J. of Power and Energy.*, vol. 229, no. 5, pp. 560–568, 2016.

[21] S. W. Chang and H. Shen, "Heat transfer of impinging jet array with web-patterned grooves on nozzle plate," *Int. J. Heat Mass Transf.*, vol. 141, pp. 129–144, 2019.

[22] M. Attalla, H. M. Maghrabie, A. Qayyum, A. G. Al-hasnawi, and E. Specht, "Influence of the nozzle shape on heat transfer uniformity for in-line array of impinging air jets," *Appl. Therm. Eng.*, vol. 120, pp. 160-169, 2017.

[23] J. Lee and S. Lee, "The effect of nozzle configuration on stagnation region heat transfer enhancement of axisymmetric jet impingement," *Int. J. Heat Mass Transf.*, vol. 43, pp. 3497–3509, 2000.

[24] A. Umit and K. Arslan, "Effects of Extended Jet Holes to Heat Transfer and Flow Characteristics of the Jet Impingement Cooling," *ASME. J. Heat Transfer.*, vol. 141, no. 8, pp. 1–14, August 2019.

[25] Y. W. Ekkad, S. V., Esposito, E. I., Kim, "Zero-cross-flow impingement via an array of differing length, extended ports," *United States Patent.*, no. US 8127553 B2, 2012.

[26] A. J. Chorin, "Numerical solution of navier-stokes equations," *Math. Comput.*, vol. 22, p. 745–762, 1968.

[27] E. Wright, A. Ahmed, Y. Yan, J. Maltson, and L. Lopez, "Experimental and Numerical Heat Transfer Investigation of Impingement Jet Nozzle Position in Concave Double-Wall Cooling Structures," *Heat Transf. Eng.*, 2021.

[28] E. Wright, A. Ahmed, Y. Yan, J. Maltson, and L. Lopez, "Experimental and Numerical Heat Transfer Investigation of Impingement Jet Nozzle Position in Concave Double-Wall Cooling Structures," *The 16th UK Heat Transfer Conference, Nottingham*, 2019.

[29] T. R. Society, P. Transactions, R. Society, C. Papers, and P. Character, "The Deferred Approach to the Limit," *Soc. R. Trans. Philos. Soc. R. Pap. Contain. Character, Phys.*, vol. 226, no. 636-646, 1927.

[30] B. E. Launder and D. B. Spalding, “Lectures in Mathematical Models of Turbulence,” *Acad. Press. London, England*, 1972.

[31] T. H. Shih, W. W. Liou, A. Shabbir, Z. Yang, and J. Zhu, “A New Eddy-Viscosity Model for High Reynolds Number Turbulent Flows-Model Development and Validation,” *Comput. Fluids*, vol. 24, no. 3, p. 227–238, 1995.

[32] D. C. Wilcox, “Turbulence Modeling for CFD,” . *DCW Ind. Inc. La Canada.*, vol. 2, pp. 103-217, 1998.

[33] F. R. Menter, “Two-Equation Eddy-Viscosity Turbulence Models for Engineering Applications,” *AIAA J.*, vol. 32, no. 2, p. 1598–1605, 1994.

[34] Y. Rao, Y. Liu, and C. Wan, “Multiple-jet impingement heat transfer in double-wall cooling structures with pin fins and effusion holes,” *Int. J. Therm. Sci.*, vol. 133, no. June, pp. 106–119, 2018.

[35] S. Spring, Y. Xing, and B. Weigand, “An Experimental and Numerical Study of Heat Transfer From Arrays of Impinging Jets With Surface Ribs,” *ASME. J. Heat Transfer.*, vol. 134, no. 8, pp. 1–11, August 2012.

[36] Y. Xing, S. Spring, and B. Weigand, “Experimental and numerical investigation of impingement heat transfer on a fl at and micro-rib roughened plate with different cross fl ow schemes,” *Int. J. Therm. Sci.*, vol. 50, no. 7, pp. 1293–1307, 2011.

[37] L. Guo, Y. Yan, and J. D. Maltson, “Performance of 2D scheme and different models in predicting flow turbulence and heat transfer through a supersonic turbine nozzle cascade,” *Int. J. Heat Mass Transf.*, vol. 55, no. 23–24, pp. 6757–6765, 2012.